ACS APPLIED ENERGY MATERIALS

May 2021
Volume 4
Number 5
pubs.acs.org/acsaem

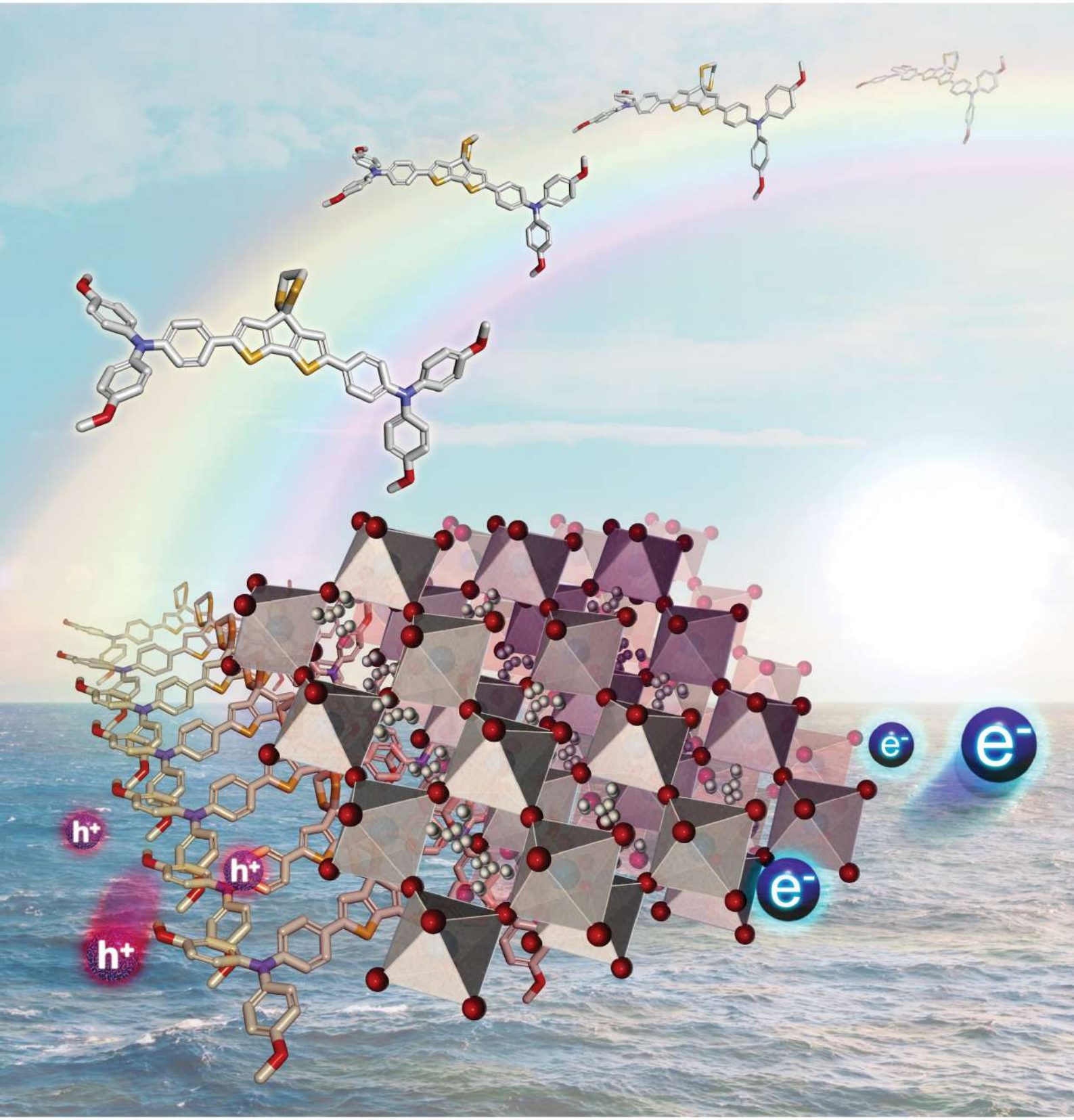

ACS Publications
Most Trusted. Most Cited. Most Read.

www.acs.org

ACS APPLIED ENERGY MATERIALS

www.acsaem.org Article

Molecularly Engineered Cyclopenta[2,1-*b*;3,4-*b*′]dithiophene-Based Hole-Transporting Materials for High-Performance Perovskite Solar Cells with Efficiency over 19%

Yan-Duo Lin,* Kun-Mu Lee,* Sheng Hsiung Chang, Tsung-Yu Tsai, Hsin-Cheng Chung, Chien-Chun Chou, Heng-Yu Chen, Tahsin J. Chow,* and Shih-Sheng Sun*

Cite This: *ACS Appl. Energy Mater.* 2021, 4, 4719−4728 Read Online

ACCESS | Metrics & More | Article Recommendations | Supporting Information

ABSTRACT: Three cyclopenta[2,1-*b*;3,4-*b*′]dithiophene (CPDT)-based organic semiconductors **LYC-1**-**LYC-3** consisting of a central dithiolane ring with triarylamine-based side groups were prepared and utilized as hole-transporting materials (HTMs) in perovskite solar cells (PSCs). Physical studies on HTM **LYC-1** indicated that it exhibits high efficiency in hole transfer and a strong hole-extraction tendency from the perovskite layer. The PSC device made with **LYC-1** as HTM showed a remarkable performance of 19.07%, which is much higher than the device based on spiro-OMeTAD (17.90%) under a similar condition. Moreover, the hydrophobic nature of **LYC-1** protects the perovskite layer effectively from moisture and, therefore, leads to its long-term stability, i.e., retains 85% of initial efficiency after operating over 1000 h. This work demonstrates that the incorporation of a dithiolane ring in the central CPDT core is an effective way of enhancing both efficiency and stability of PSC devices.

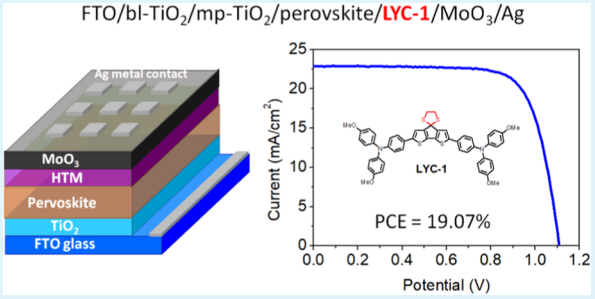

KEYWORDS: *perovskite, cyclopentadithiophene, hole-transporting material, long-term stability, carbazole*

INTRODUCTION

Perovskite solar cells (PSCs) have drawn considerable attention due to their outstanding physical and optoelectronic properties such as the long carrier-diffusion length, intense panchromatic light absorption, and high charge-carrier mobility.[1−4] In less than 10 years, PSCs have experienced a remarkable advancement in their power conversion efficiencies (PCEs) from 3.8% to over 25%, rivaling the commercial silicon solar cells.[5−10] A typical device configuration of PSCs is composed of a transparent electrode, an electron transporting layer (ETL), a perovskite absorption layer, a hole-transporting layer, and a back contact metal electrode. A highly efficient PSC is usually archived by introducing a hole-transporting material (HTM) between the perovskite layer and the metal electrode to induce hole extraction and suppress the charge recombination at the interface. Nowadays, the most popular HTM employed in PSCs is 2,2′,7,7′-tetrakis-(*N*,*N*-di-*p*-methoxyphenyl-amine)-9,9′-spirobifluorene (spiro-OMeTAD) that can afford a conversion efficiency higher than 20%.[11] The major drawbacks of spiro-OMeTAD are its tedious synthesis and the purification procedure as well as its relatively low charge-carrier mobility.[12] These drawbacks become a major obstacle for large-scale applications.[13] Therefore, great efforts have been spent in recent years on seeking alternative materials with the aim of surpassing the performance of spiro-OMeTAD. For inorganic materials such as CuI and CuSCN, the efficiencies of the PSCs based on them are still lower than those obtained using either spiro-OMeTAD or polytriarylamine (PTAA) polymers.[14,15] Compared with polymeric materials, small molecules possess certain advantages in terms of ease synthesis, convenient purification, high purity, precise molecular weight, and handy batch-to-batch reproduction.[16,17] In this regard, a variety of organic small molecules have been designed and employed as HTMs in PSCs, such as spiro-type compounds, truxenes, benzotrithiophenes, bifluorenylidenes, azahelicenes, bimesitylenes, and their derivatives.[12,18−28] Despite the rapid growth of small-molecule-based HTMs, it is still crucial to understand the factors that govern the correlation between the molecular structure and the device performance.

Organic materials containing fused thiophene units are commonly used as organic semiconductors.[29] The electron-rich nature of sulfur and the rigid planar π-conjugated framework can enhance the hole mobility through an intermolecular overlap of $\pi-\pi$ clouds in the solid state.[30,31]

Received: January 31, 2021
Accepted: April 8, 2021
Published: April 21, 2021

https://doi.org/10.1021/acsaem.1c00328
ACS Appl. Energy Mater. 2021, 4, 4719−4728

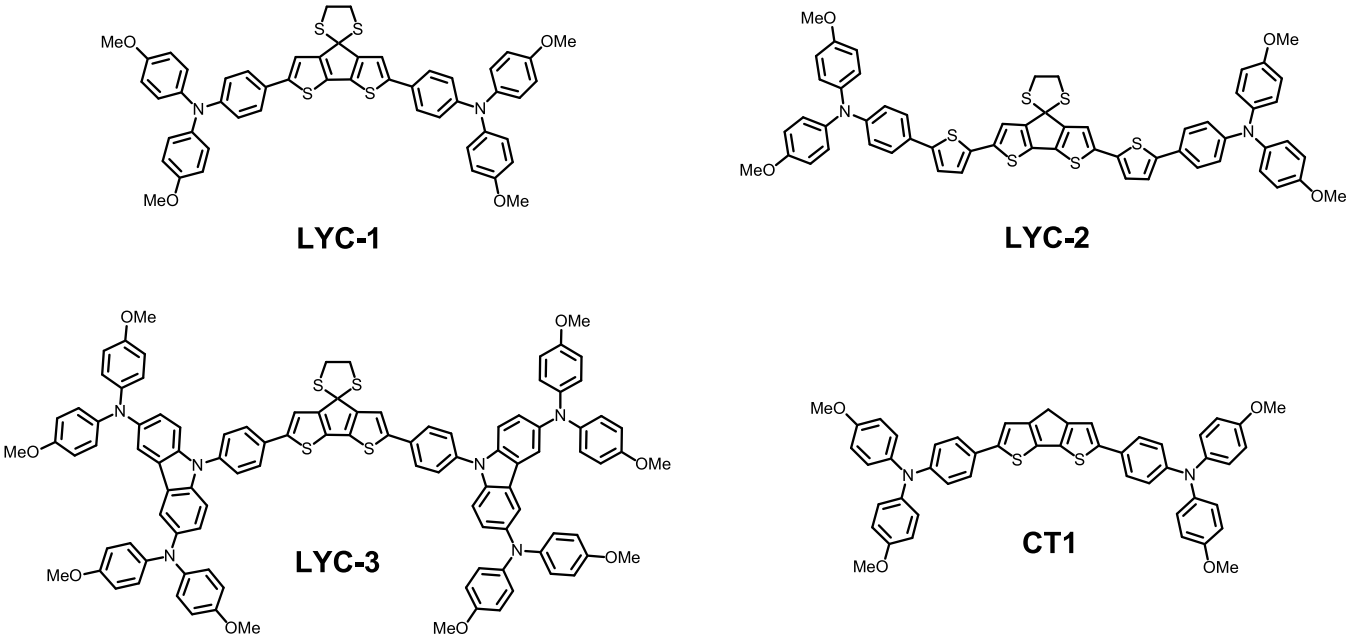

Figure 1. Chemical structures of **LYC** HTMs and **CT1**.

Scheme 1. Synthetic Route for LYC Series

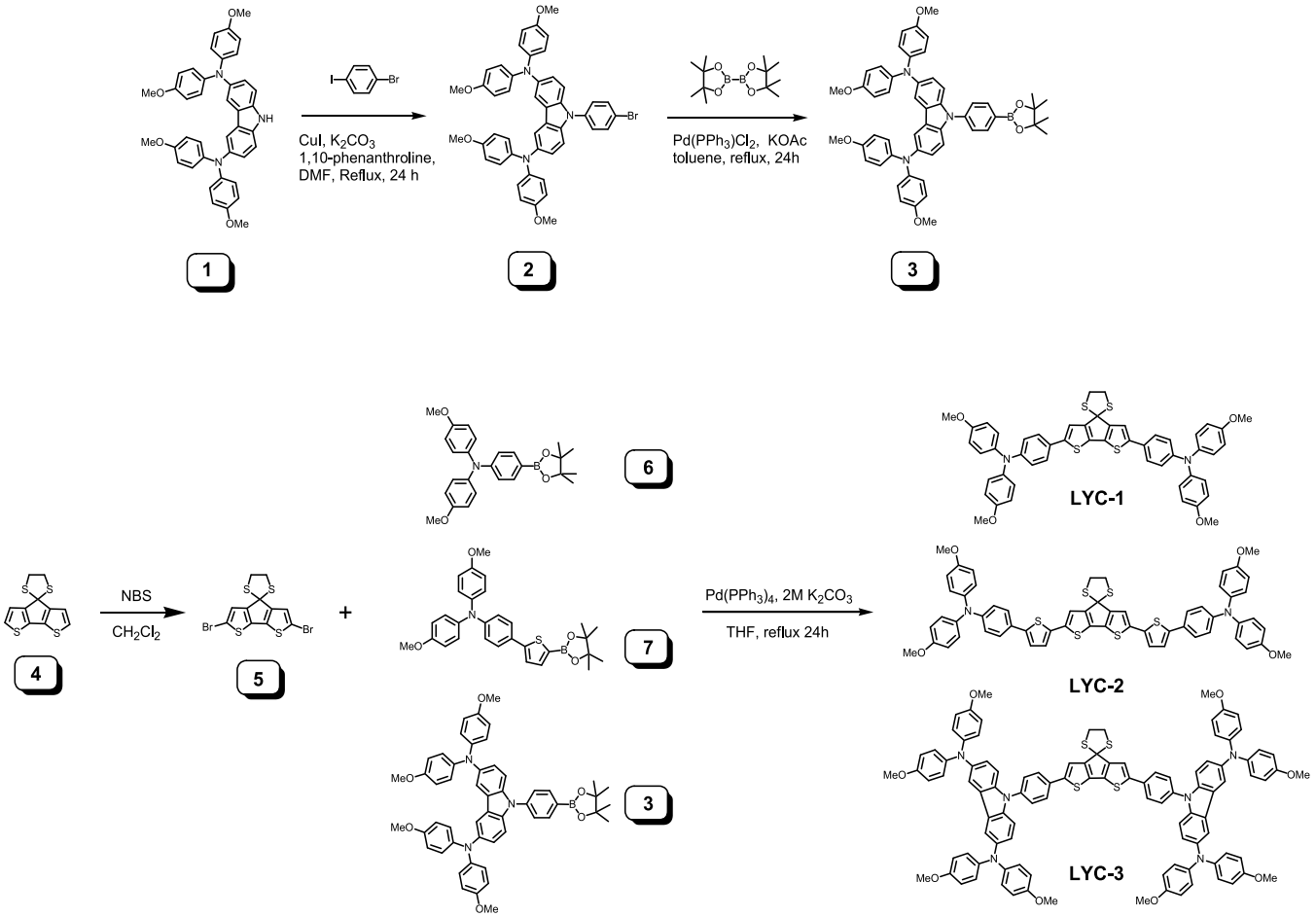

Not only the $\pi-\pi$ interaction, the S···S interaction is also beneficial to charge transport due to the electronic softness of the sulfur atoms and, thus, an increase of effective overlapping. These effects have been demonstrated in several thiophene-fused aromatic compounds.[32,33] Among them, cyclopenta[2,1-*b*;3,4-*b*′]dithiophene (CPDT) and its derivatives have been employed as building blocks in preparing semiconducting materials for various optoelectronic devices,[34−37] although the

https://doi.org/10.1021/acsaem.1c00328
ACS Appl. Energy Mater. 2021, 4, 4719−4728

properties of small molecules containing CPDT used for PSCs have received much less attention.[12,38−42]

Herein, we present our studies on a new class of hole-transporting materials by incorporating a dithiolane unit into a CPDT moiety endowed with arylamines and diphenylamine-substituted carbazole and showcase their effectiveness as HTMs for highly efficient and stable PSCs. The structures of **LYC-1**, **LYC-2**, and **LYC-3** are shown in Figure 1. To the best of our knowledge, compounds containing a dithiolane moiety used as the HTMs in PSCs have never been examined. The spiro-dithiolane ring of CPDT derivatives with the two additional sulfur atoms on the central core may enhance good intermolecular packing via S···S interactions, thereby inducing a preferable packing arrangement for increasing charge transportation.[43] The optoelectronic and electrochemical properties of these three new HTMs were systemically investigated. Theoretical calculations were conducted to obtain the energy levels and electronic configurations. By comparison with the previously reported compound **CT1** without the dithiolane ring,[42] we were able to investigate the influences of these pendant groups on the physical and chemical properties and their contributions to the photovoltaic performance. The cell performance based on **LYC-1**, in particular, showed an excellent power conversion efficiency (PCE) of 19.07%, notably better than the one based on standard spiro-OMeTAD (17.90%) and previously reported **CT1** (17.71%) without the dithiolane unit in the bridged head of fused thiophene[42] under the same condition. Not only showing excellent device performance, the device base on the **LYC-1** also showed outstanding long-term stability in an ambient atmosphere in the dark over 1000 h. These findings suggest that dithiolane-based CPDT materials are promising organic semiconductors for highly efficient PSCs.

RESULTS AND DISCUSSION

The synthesis of **LYC** HTMs is illustrated in Scheme 1 and the detailed experimental procedures are summarized in the Supporting information. The synthesis of compound **3** has been recently reported.[42,44] Bromination of 1,3-dithiolane **4**[45] by *N*-bromosuccinimide (NBS) yielded the dibromo derivative **5**. The final **LYC** molecules were obtained by following the Suzuki coupling reactions of **5** with *p*-methoxytriphenylamine (**6**), *p*-methoxytriphenylamine-substituted thiophene (**7**),[39] and *p*-methoxydiphenylamine carbazole-based pinacolboronates (**3**), respectively, to give the disubstituted derivatives **LYC-1**, **LYC-2**, and **LYC-3** in good yields. The identities of all compounds were fully confirmed by $^{1}H/^{13}C$ NMR spectroscopy and high-resolution mass spectrometry.

Crystals of **LYC-1** suitable for X-ray crystallographic studies were grown from CH_2Cl_2/hexane solutions by slow solvent evaporation under ambient environments. The structure is shown in Figure S1 and the detailed crystallographic data can be found in Table S1. Compound **LYC-1** crystallizes in a triclinic $P\bar{1}$ space group. The CPDT tricyclic core is planar, which shows a slight twist from the adjacent phenyl rings with dihedral angles in the range of 5.4−18.4°. Such π-extended planar skeleton improves face to face $\pi-\pi$ overlap, facilitating charge transport and expecting to promote the hole mobility.[46]

The photophysical characteristics of **LYC** HTMs in chlorobenzene solutions are evaluated, as shown in Figure 2, and the corresponding data are collected in Table 1. The absorption maximum in the visible region depends on the nature of the substituent. Compounds **LYC-1**, **LYC-2**, and

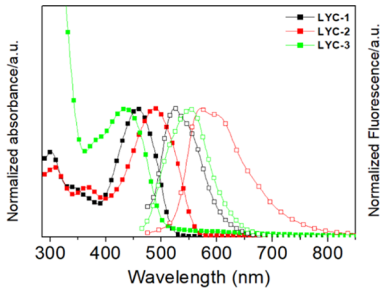

Figure 2. Normalized absorption (■) and emission (□) spectra of **LYC** HTMs in chlorobenzene solutions.

LYC-3 exhibit maximum absorption bands at 457, 489, and 435 nm, respectively. The absorption maximum of **LYC-3** is blue-shifted compared to those of **LYC-1** and **LYC-2**. The absorption spectrum of **LYC-2** exhibits a bathochromic shift of 32 nm compared to **LYC-1**, ascribed to the extended conjugation length of **LYC-2** by introducing the thiophenylene group in the structure. The same trend was observed in the fluorescence spectra (λ_f = 524 nm for **LYC-1** and λ_f = 570 nm for **LYC-2**). The degree of conjugation is obviously a determining factor in the observed order of absorption and fluorescence maxima. Moreover, the larger Stokes shift of **LYC-3** (4840 cm^{-1}) between the absorption and fluorescence spectra with respect to **LYC-1** (2761 cm^{-1}) and **LYC-2** (2906 cm^{-1}) revealed a significant structural distortion between the ground state and the excited state for **LYC-3**. The highest occupied molecular orbital (HOMO)−lowest unoccupied molecular orbital (LUMO) energy gaps (E_{0-0}) of **LYC-1**, **LYC-2**, and **LYC-3** were determined to be 2.50, 2.30, and 2.55 eV, respectively, from the normalized absorption and emission intersection.

The computational studies were performed using density functional theory (DFT) and time-dependent DFT (TDDFT) calculations on the level of B3LYP hybrid functional and the 6-31G(d,p) basis set to gain insights into the frontier molecular orbitals and the energy states. The optimized geometries and the electron distribution of **LYC** series are displayed in Figure 3. The LUMOs of **LYC** series are mostly located on the 1,3-dithiolane core and the neighboring phenyl or thienyl rings, whereas the HOMOs of both **LYC-1** and **LYC-2** are broadly delocalized over the TPA-donor and spacer moieties. In contrast, the HOMO electron density of **LYC-3** is primarily localized on the carbazole-diphenylamine moiety. The HOMO/LUMO energy levels were calculated to be −4.27/−1.47 eV for **LYC-1**, −4.34/−1.85 eV for **LYC-2**, and −4.27/−1.90 eV for **LYC-3**, respectively. Accordingly, the energy gaps of **LYC-1**, **LYC-2**, and **LYC-3** are 2.80, 2.49, and 2.37 eV, respectively. Furthermore, the absorption transitions of **LYC** series were calculated by TDDFT, and the relevant results for the calculated absorption spectra are shown in Figure S2. The vertical excitation energies and oscillator strengths *f* for the lowest 10 singlet−singlet excitations are summarized in Table S2. It is noticed that the simulated absorption spectra of **LYC** HTMs show two absorption peaks. The calculated spectral profiles comply well with the experimental results (Figure 2). The lowest excitation bands of **LYC** series are assigned to the transition from the HOMO → LUMO levels. The thermal stabilities of **LYC** HTMs were determined by thermogravimetric analysis (TGA). Compounds **LYC-1**, **LYC-2**, and **LYC-3** possess high decomposition temperatures at 304, 316, and

https://doi.org/10.1021/acsaem.1c00328
ACS Appl. Energy Mater. 2021, 4, 4719−4728

Table 1. Photophysical and Electrochemical Data of LYC HTMs

HTM	λ_{abs} (nm),[a] $\varepsilon \times 10^{-4}$ (M^{-1} cm^{-1})	λ_f[a] (nm)	$\Delta\upsilon_{st}$[b] (cm^{-1})	E_{HOMO}[c] (eV)	E_{0-0}[d] (eV)	E_{LUMO}[e] (eV)	I_p[f] (eV)	E_{HOMO}[g] (eV)	E_{LUMO}[g] (eV)
LYC-1	457, 5.37	524	2761	−5.25	2.50	−2.75	−5.17	−4.27	−1.47
CT1[h]	437, 5.92	502	2963	−5.17	2.57	−2.60	−5.00	−4.24	−1.31
LYC-2	489, 6.34	570	2906	−5.29	2.30	−2.99	−5.22	−4.34	−1.85
LYC-3	435, 5.19	551	4840	−5.24	2.55	−2.69	−5.19	−4.27	−1.90
spiro-OMeTAD	389, 18.37	428	2342	−5.22	3.03	−2.19	−5.14	−4.24	−2.23

[a]Measured in chlorobenzene solutions. [b]$\Delta\upsilon_{st} = \upsilon_{abs} - \upsilon_f$. [c]Determined from the differential pulse voltammetry (DPV) results. [d]Obtained from the intersection of normalized absorption and fluorescence spectra. [e]Estimated by $E_{HOMO}-E_{0-0}$. [f]Ionization potentials measured by the photoelectron spectroscopy of films in air. [g]Calculated values by time-dependent density functional theory (TDDFT). [h]Taken from ref 42.

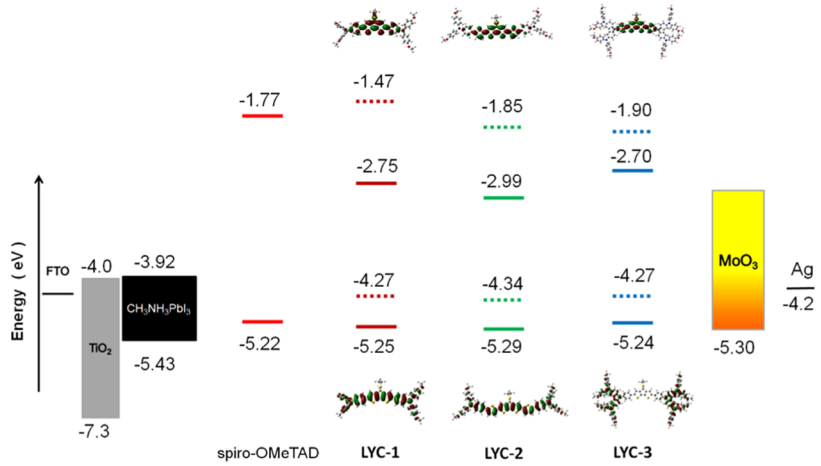

Figure 3. Energy level diagram of the corresponding HTMs and related materials in a device. Calculated HOMO and LUMO values are presented as dashed lines.

392 °C, respectively. The high thermal stability suggests that all materials are suitable for PSC applications (Figure S3).

Energy level matching of HTMs and perovskite is an important factor to achieve high-performance PSCs. In this regard, we have performed cyclic voltammetry (CV) (Figure S4) and differential pulse voltammetry (DPV) (Figure 4)

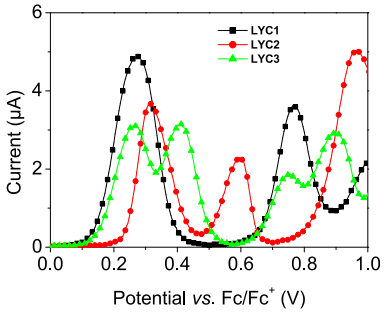

Figure 4. Differential pulse voltammograms of **LYC** series measured in tetrahydrofuran (THF) solutions.

experiments to estimate the energy levels. The electrochemical data are collected in Table 1. Figure 3 illustrates the energy levels of perovskite and related materials. The first oxidation potentials are −5.25, −5.29, and −5.24 eV for **LYC-1**, **LYC-2**, and **LYC-3**, respectively. The HOMO levels of **LYC** HTMs are sufficiently higher than that of the perovskite to ensure sufficient driving force for hole extraction. The LUMO levels of **LYC-1**, **LYC-2**, and **LYC-3** are −2.75, −2.99, and −2.67 eV, respectively. These values are significantly higher than that of the conduction band of perovskite to suppress the back electron transfer from perovskite to the counter electrode.

To evaluate the solid-state optoelectronic properties, the energy levels of **LYC** series were investigated by measuring their photoelectron spectra in air (Figure 5). The data are also

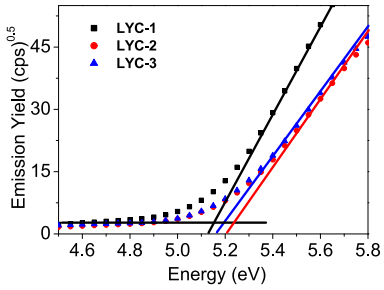

Figure 5. Photoelectron spectra of **LYC** series in air.

compiled in Table 1. The trend of HOMO values for **LYC** series obtained by photoelectron spectroscopy is consistent with the computational results by DFT and the measurements by DPV.

The space-charge-limited current (SCLC) method was employed to evaluate the hole-transporting properties of **LYC** series (Figure 6). High hole mobility facilitates hole extraction and is beneficial for improving the fill factor (FF) of the PSC devices. **LYC-1** exhibited a higher hole mobility (7.53×10^{-4} cm^2 V^{-1} s^{-1}) than those of **LYC-2** (3.06×10^{-4} cm^2 V^{-1} s^{-1}) and **LYC-3** (2.34×10^{-5} cm^2 V^{-1} s^{-1}). The higher hole mobility of **LYC-1** when compared to **LYC-2** and **LYC-3** is tentatively attributed to the difference in their chemical

https://doi.org/10.1021/acsaem.1c00328
ACS Appl. Energy Mater. 2021, 4, 4719−4728

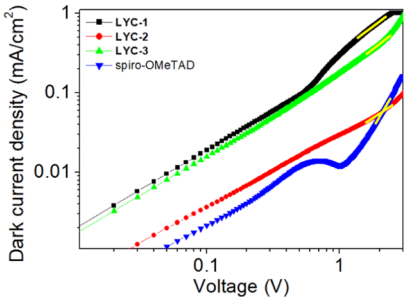

Figure 6. Space-charge limitation of current in the $J-V$ characteristics of the device with different HTMs.

structures. According to our previous studies, a shorter π-conjugated system provides better $\pi-\pi$ interactions for holes to hop through molecules.[25] The extended π-conjugation side arms of HTMs may penetrate into those of neighboring molecules and lead to partial $\pi-\pi$ interaction that can consequently interfere with the preferred charge-transport pathways. In addition, the thin-film morphology of **LYC-1** showed a more homogeneous and uniform surface when compared with **LYC-2** (vide infra). The smoother HTM surface is beneficial for hole extraction and transport in the film, resulting in better photovoltaic performance. Lower hole mobility of 3.58×10^{-4} cm^2 V^{-1} s^{-1} was obtained for spiro-OMeTAD in comparison to that of **LYC-1**. In addition, the hole mobility of compound **CT1** reported in our previous work is 3.21×10^{-4} cm^2 V^{-1} s^{-1}.[42] Clearly, the close stacking interactions between the HTMs induced by the additional intermolecular S···S interactions in the dithiolane-ring-based **LYC-1** is responsible for a higher hole mobility than that of **CT1**.[46,47] The high hole mobility for **LYC-1** is expected to promote the performance of PSCs.

To gain insights into the hole-extraction capability, we evaluated the hole-extraction ability by examining the steady-state photoluminescence (PL) spectra and time-resolved photoluminescence (TRPL). The PL spectra of perovskite in **LYC** series and spiro-OMeTAD is shown in Figure 7a. It can be seen that there is a strong PL signal at 770 nm from the perovskite film without HTMs. However, the PL of bilayered $MAPbI_3$/HTMs exhibited a significant quenching effect with respect to that of the pristine perovskite film, indicating effective hole extraction. The degree of PL quenching of perovskite deposited on either **LYC-2** or **LYC-3** was about ~80%, while that deposited on **LYC-1** was nearly 95%. The difference indicates that **LYC-1** displayed the most efficient charge-extraction effect among the **LYC** series, which is consistent with its highest hole mobility. Figure 7b shows the decay traces of TRPL. By fitting with a two-component exponential model, the average PL lifetime of a pristine perovskite film, perovskite/**LYC-1**, perovskite/**LYC-2**, perovskite/**LYC-3**, and perovskite/spiro-OMeTAD were determined to be 31.77, 16.57, 19.56, 21.39, and 17.37 ns, respectively (Table S3). As expected, the PL lifetime significantly decreased in HTM-covered perovskite films. In addition, an **LYC-1**-coated perovskite film exhibited the shortest average lifetime among the **LYC** series, indicating that **LYC-1** has a superior carrier-extraction ability.

A smooth and dense layer of HTM covered on top of the perovskite crystals is critical to boost the efficiency of PSCs. The surface morphologies of **LYC** series film spin-coated on perovskite were characterized by atomic force microscopy (AFM). The three-dimensional (3-D) morphologies of **LYC**s are shown in Figure 8. The films of **LYC-1**, **LYC-2**, and **LYC-3** showed root-mean-square (RMS) roughness values of 5.0, 6.9, and 8.5 nm, respectively. A smooth surface of an **LYC-1**-covered film suggests that this HTM is likely to display a better property, such as forming a better contact with the perovskite layer to reduce charge leakage. The smooth **LYC-1** film would lead to a higher J_{sc} value and a good overall PCE. To understand interfacial contact of the **LYC** series film, we examined the contact angle of water droplets and determined the hydrophobicity of the HTMs. As shown in Figure S5, the contact angles measured for casted **LYC-1**, **LYC-2**, **LYC-3**, and spiro-OMeTAD were 78, 72, 63, and 70°, respectively. The **LYC-1** film showed higher hydrophobicity than those of **LYC-2** and **LYC-3** films so that it is more effective for the **LYC-1** film to prevent water penetration into the perovskite surface and thus improve the long-term stability of devices. X-ray diffraction spectroscopy was employed to investigate the molecular arrangement of the solid films (Figure S6). The broad amorphous diffraction pattern of all films clearly showed a noncrystalline amorphous nature of **LYC** HTMs.

The PSC devices with a configuration of FTO/blocking layer-TiO_2/mp-TiO_2/perovskite/HTM/MoO_3/Ag were fabricated to realize the potential of **LYC** materials as suitable HTMs. Addition of the MoO_3 layer between the HTMs and Ag is known to enhance the PCE in PSCs.[42] Detailed device preparation is described in the Supporting Information. For comparison, the photovoltaic performance of PSCs fabricated using spiro-OMeTAD was also included. Figure 9 shows a cross-sectional scanning electron microscopy (SEM) image of an optimum device employing **LYC-1** as the HTM. The HTM layer can be clearly distinguished from the perovskite layer and

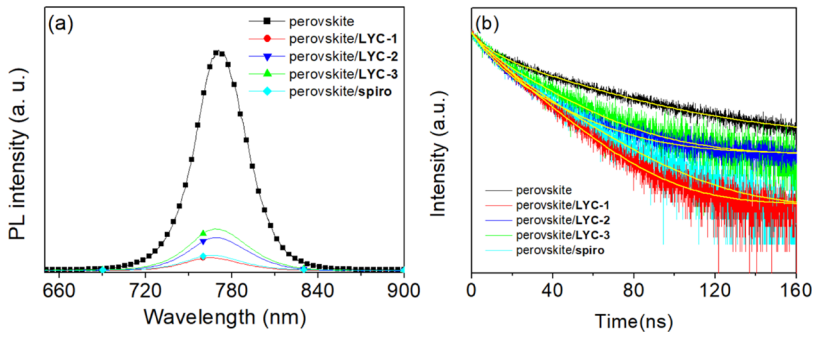

Figure 7. (a) PL spectra of perovskite films. (b) Decay traces of time-resolved photoluminescence of the pristine perovskite film and the perovskite film covered by different HTMs.

https://doi.org/10.1021/acsaem.1c00328
ACS Appl. Energy Mater. 2021, 4, 4719−4728

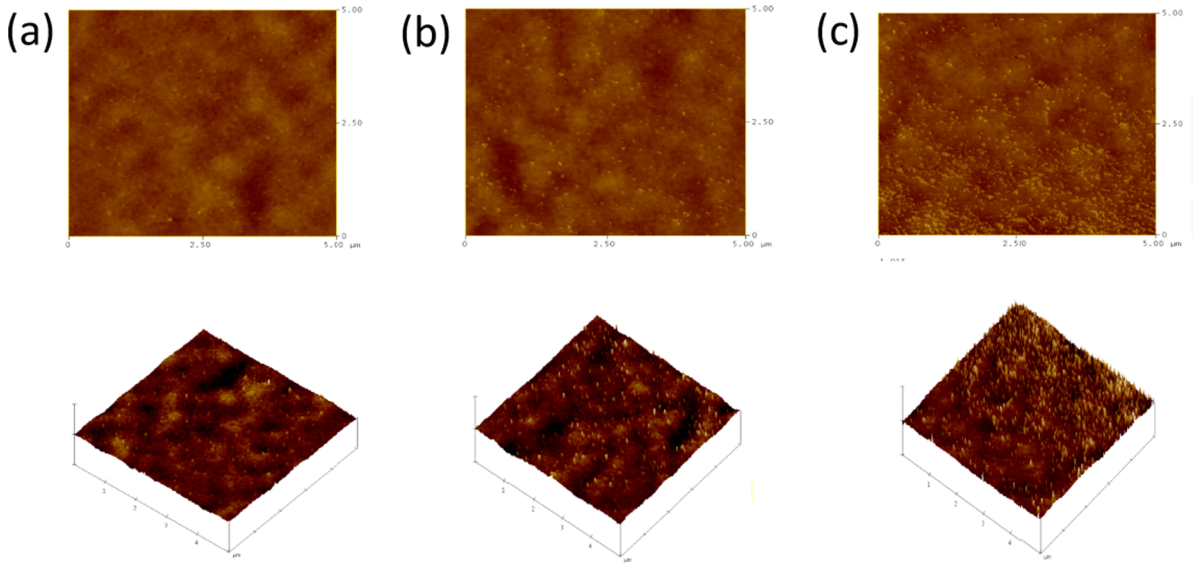

Figure 8. 3-D surface plots of HTM films by AFM (a) **LYC-1**, (b) **LYC-2**, and (c) **LYC-3**.

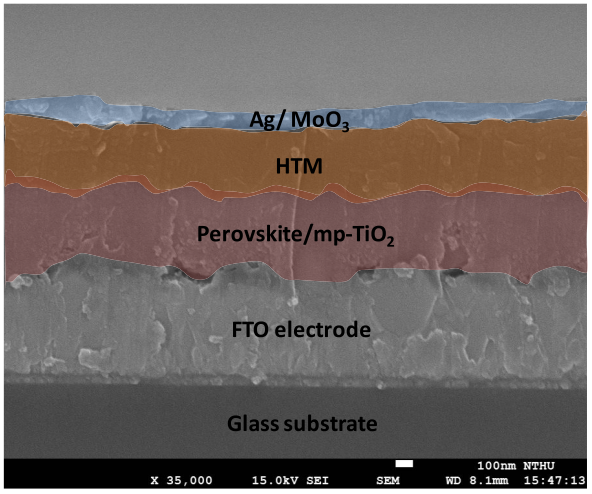

Figure 9. SEM cross-sectional image of the **LYC-1**-based device.

the Ag electrode. The optimized film thickness of HTM is roughly 400 nm. The current density−voltage (J−V) plots under AM 1.5G illumination with reverse scans are displayed in Figure 10, and the device performance data are collected in Table 2.

The optimized **LYC-1**-based PSCs exhibited a high PCE of 19.07%, with an open-circuit voltage (V_{oc}) of 1.11 V, a short-circuit current density (J_{sc}) of 22.88 mA cm^{-2}, and a fill factor (FF) of 0.751. Such a performance is better than that of PSCs based on spiro-OMeTAD fabricated under a similar condition, with V_{oc} of 1.09 V, J_{sc} of 22.87 mA cm^{-2}, and FF of 0.718, leading to a PCE of 17.90% (Figure 10a). It is noteworthy that the J_{sc} value of **LYC-1** is comparable to that of spiro-OMeTAD, but the V_{oc} and FF values are higher due to the good hole-extraction and transport ability, as well as the excellent film morphology, indicating that **LYC-1** can act as a more effective HTM for PSCs. After introducing a thiophene ring between the triphenylamine moieties and the CPDT core as the donor group, the **LYC-2**-based cell showed a lower PCE of 17.67%, together with V_{oc} of 1.07 V, J_{sc} of 22.29 mA cm^{-2},

Table 2. Device Performances with Different HTMs

HTM	scan direction	V_{oc} (V)	J_{sc} (mA cm^{-2})	FF	PCE (%)
LYC-1	reverse	1.11	22.88	0.751	19.07
	forward	1.03	22.11	0.747	17.01
CT1[a]	reverse	1.03	22.45	0.766	17.71
	forward	1.03	22.28	0.672	15.42
LYC-2	reverse	1.07	22.29	0.738	17.60
	forward	1.03	21.8	0.641	14.39
LYC-3	reverse	1.07	21.76	0.701	16.32
	forward	1.03	21.49	0.661	14.63
spiro-OMeTAD	reverse	1.09	22.87	0.718	17.90
	forward	1.08	23.09	0.68	16.87

[a]Taken from ref 42.

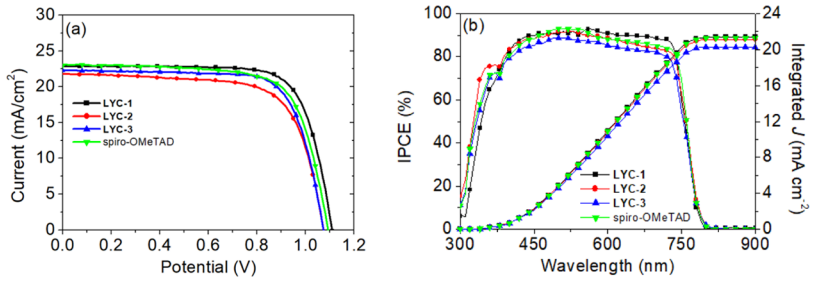

Figure 10. (a) Plot of J−V curves and (b) incident photon to current conversion efficiency (IPCE) spectra of the perovskite solar cells using **LYC** series and spiro-OMeTAD as the HTMs.

https://doi.org/10.1021/acsaem.1c00328
ACS Appl. Energy Mater. 2021, 4, 4719−4728

and FF of 0.738. When the triphenylamine-terminated groups in **LYC-1** are replaced with carbazole groups, an obvious decrease of V_{oc}, J_{sc}, and FF is observed. As a result, the **LYC-3**-based cell showed a relatively low efficiency of 16.38% with V_{oc} of 1.07 V, J_{sc} of 21.76 mA cm^{-2}, and FF of 0.701. The higher V_{oc} and FF values for cells fabricated with **LYC-1** than those with **LYC-2** and **LYC-3** are attributed to an overall effect of higher hole mobility, hole extraction, and the better film quality of **LYC-1** according to SCLC, P,L and AFM results. In spite of the similar redox potentials among **LYC** series, the device based on **LYC-1** showed a higher J_{sc} value with respect to **LYC-2** and **LYC-3**, therefore it indicates a more efficient hole injection between the perovskite and the HTM layer. It is clearly found that the photovoltaic performances for **LYC** series were significantly affected by the terminated group on the CPDT core. Nevertheless, a hysteresis could be observed between the forward and reverse scans based on these new HTMs (Figure S7). The incorporation of a dithiolane ring on the CPDT core leads to a lower HOMO energy level and better hole mobility of **LYC-1** that is responsible for a remarkably high PCE of 19.07% in comparison to **CT1** with a PCE of 17.71%.[42] To scrutinize the reproducibility of the results, we tested 40 devices prepared independently (Figure S8). A histogram on performance variations of the PSCs based on **LYC** series is shown in Figure 11. The averaged PCEs of

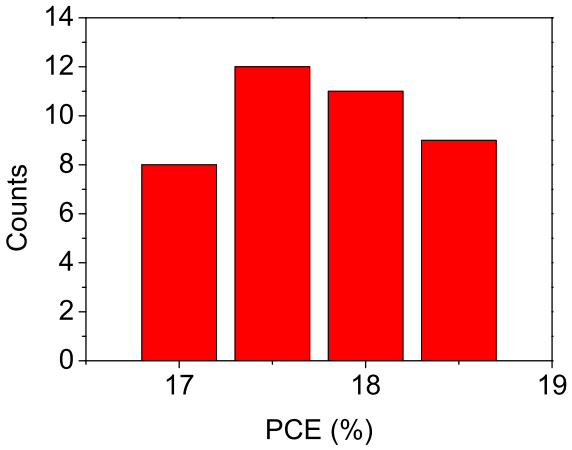

Figure 11. Histogram of PCE for 40 devices based on **LYC-1** HTM.

devices using **LYC-1**, **LYC-2**, and **LYC-3** achieved the values 18.31, 16.86, and 15.83%, respectively, under standard AM 1.5G illumination. To evaluate the potential of the three dithiolane-incorporated CPDT-based small-molecule HTMs and spiro-OMeTAD for dopant-free PSCs, the PSC devices without hygroscopic dopants were fabricated. The $J-V$ curves of **LYC** series and spiro-OMeTAD are shown in Figure S9, and their detailed photovoltaic parameters are summarized in Table S4. The PSCs using the newly prepared dopant-free dithiolane-incorporated CPDT-based HTMs and spiro-OMeTAD all show significantly low photovoltaic performance. Devices with **LYC-1**, **LYC-2**, **LYC-3**, and spiro-OMeTAD yielded efficiencies of 4.76, 4.69, 2.60, and 0.17%, respectively, under reverse scan.

The incident photon to current conversion efficiency (IPCE) spectra of the perovskite devices are presented in Figure 10b. The IPCE spectra for all HTMs exhibit a broad spectral coverage from 400 to 700 nm. The integrated photocurrent densities are 21.38, 21.12, 20.29, and 21.27 mA cm^{-2} for devices with **LYC-1**, **LYC-2**, **LYC-3**, and spiro-OMeTAD, respectively, which are in good agreement with J_{sc} determined from the $J-V$ curve. The lower performance in IPCE for **LYC-3** can be ascribed to the lower hole mobility and less efficient hole-extraction ability. Moreover, the stabilized PCE and photocurrent density at maximum power point (0.82 V) conditions was measured as a function of time (Figure 12).

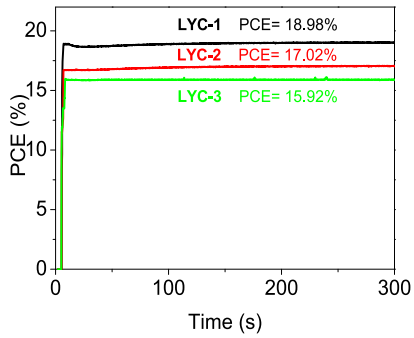

Figure 12. Stabilized maximum power output of a device with different HTMs.

The **LYC**-based devices show stable photocurrent density and yield a PCE of 18.98, 17.02, and 15.92% for **LYC-1**, **LYC-2**, and **LYC-3**, respectively, after the measurements of 300 s. It was found that **LYC**-based devices showed very stable photovoltaic performance.

The long-term stability of PSCs is highly critical for commercial application. Therefore, we evaluate the stability of **LYC**-based PSCs under an ambient atmosphere with 40% relative humidity at 30 °C without encapsulation over 1000 h in a dark condition. As shown in Figure 13, the **LYC-1**-based devices show good stability and maintain ∼85% of their highest efficiency with small variations in V_{oc}, J_{sc}, and FF after 1000 h storage in the dark. However, for **LYC-2**- and **LYC-3**-based devices, the PCE degraded to about ∼80% over the period of aging time. In comparison, a 25% efficiency drop of the spiro-OMeTAD-based devices was observed. The great long-term stability of **LYC-1**-based PSCs is attributed to the better hydrophobic property and the film homogeneity of **LYC-1** that covers the top of the perovskite material.

Electrochemical impedance spectroscopy (EIS) was conducted at a bias of 0.9V under one sun illumination to reveal insights on the interfacial charge-transport process in PSCs. The EIS Nyquist plots with various HTMs are presented in Figure 14. The equivalent circuit models were utilized to obtain the fitting results. The arc in the low-frequency region is associated with the charge recombination resistance (R_{rec}) of the HTMs/perovskite interface. According to the fitting results, the R_{rec} value for **LYC-1**-based PSC is larger than those of devices using other **LYC** series and spiro-OMeTAD. The results suggest a slower recombination process for **LYC-1**-based PSCs, leading to better performance among the PSCs tested.

CONCLUSIONS

In this work, three electron-rich CPDT-based HTMs incorporating a dithiolane ring at the central core with various substituents were prepared and successfully employed in PSCs. The optical and electrochemical properties of **LYC** series were thoroughly analyzed. The HOMO and LUMO energy levels and their redox potentials were found suitable for the

https://doi.org/10.1021/acsaem.1c00328
ACS Appl. Energy Mater. 2021, 4, 4719−4728

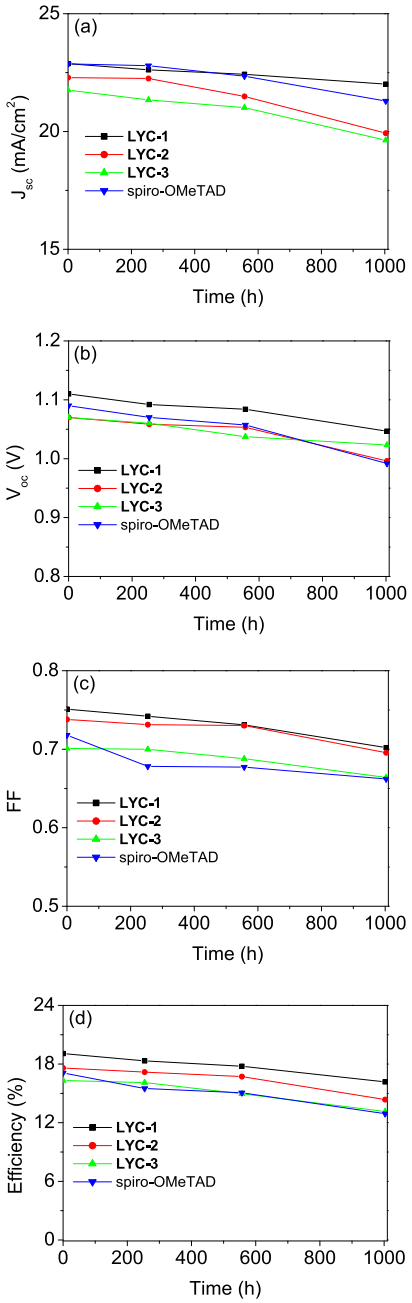

Figure 13. Stability test (a) J_{sc}, (b) V_{oc}, (c) FF, and (d) PCE of PSCs containing **LYC** series and spiro-OMeTAD as HTMs.

operation of PSCs. The highest hole mobility was obtained with **LYC-1** (7.53×10^{-4} cm^2 V^{-1} s^{-1}) among all **LYC** HTMs and higher than that of spiro-OMeTAD and **CT1**. Photoluminescence experiments showed the PL signal of the **LYC-1**/perovskite bilayer is more effectively quenched than the other two **LYC** HTMs and spiro-OMeTAD, indicating a better hole-extraction ability of **LYC-1**. The perovskite solar cell made with **LYC-1** exhibited a remarkable PCE of 19.07%, significantly higher than those made with **LYC-2**, **LYC-3**, and spiro-OMeTAD under a similar condition. This is mainly attributed to its higher hole mobility, faster charge collection efficiency, and the formation of a more uniform capping layer on top of perovskite. Furthermore, in comparison with **CT1** (17.71%) HTM without a dithiolane ring, the **LYC-1** exhibits better performance. Moreover, the **LYC-1** based device also

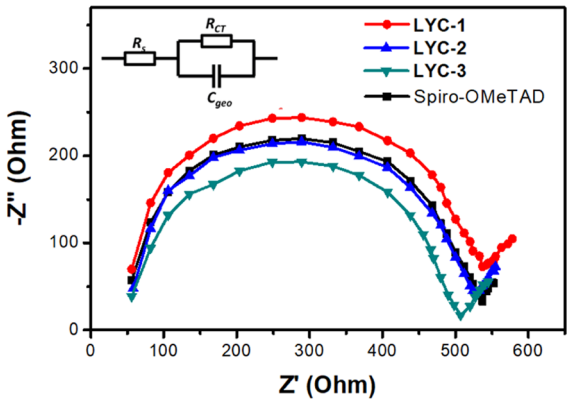

Figure 14. EIS Nyquist plots for PSCs based on **LYC-1**, **LYC-2**, **LYC-3**, and spiro-OMeTAD.

shows better long-term stability under an ambient condition with a humidity of 40%. The current work shows that the dithiolane-incorporated CPDT structure can be a promising building block for developing highly efficient HTMs in PSCs.

■ ASSOCIATED CONTENT

Supporting Information

The Supporting Information is available free of charge at https://pubs.acs.org/doi/10.1021/acsaem.1c00328.

Experimental details, synthesis of CPDT-based HTMs, NMR analysis, the crystal structure, computational data, device fabrication results, and physical measurement data including TGA curves, PXRD, and water contact angles (PDF)

■ AUTHOR INFORMATION

Corresponding Authors

Yan-Duo Lin − *Department of Chemistry, Soochow University, Taipei 11102, Taiwan;* orcid.org/0000-0002-1570-5842; Email: ydlin@scu.edu.tw

Kun-Mu Lee − *Department of Chemical and Materials Engineering and Center for Green Technology, Chang Gung University, Taoyuan 33302, Taiwan; Division of Neonatology, Department of Pediatrics, Chang Gung Memorial Hospital, Taoyuan 33305, Taiwan;* orcid.org/0000-0002-5911-9386; Email: kmlee@mail.cgu.edu.tw

Tahsin J. Chow − *Department of Chemistry, Tunghai University, Taichung 40704, Taiwan; Institute of Chemistry, Academia Sinica, Taipei 11529, Taiwan*; Email: tjchow@chem.sinica.edu.tw

Shih-Sheng Sun − *Institute of Chemistry, Academia Sinica, Taipei 11529, Taiwan;* orcid.org/0000-0001-5515-5059; Email: sssun@chem.sinica.edu.tw

Authors

Sheng Hsiung Chang − *Department of Physics, Chung Yuan Christian University, Taoyuan 32023, Taiwan;* orcid.org/0000-0003-1488-1649

Tsung-Yu Tsai − *Department of Chemistry, Soochow University, Taipei 11102, Taiwan*

Hsin-Cheng Chung − *Department of Applied Chemistry, National Chiayi University, Chiayi 60004, Taiwan*

Chien-Chun Chou − *Department of Applied Chemistry, National Chiayi University, Chiayi 60004, Taiwan*

https://doi.org/10.1021/acsaem.1c00328
ACS Appl. Energy Mater. 2021, 4, 4719−4728

Heng-Yu Chen − *Department of Applied Chemistry, National Chiayi University, Chiayi 60004, Taiwan*

Complete contact information is available at: https://pubs.acs.org/10.1021/acsaem.1c00328

Notes

The authors declare no competing financial interest.

■ ACKNOWLEDGMENTS

The authors acknowledge the support from the Academia Sinica (Grant No. AS-SS-108-02). Y.-D. L. thanks the Ministry of Science and Technology (Grant No. MOST 109-2113-M-031-007-) for research support. K.-M. L. thanks the Ministry of Science and Technology, Taiwan (Grant No. MOST 108-2628-E-182-003-MY3), the Chang Gung University (QZRPD181), and the Chang Gung Memorial Hospital, Linkou, Taiwan (CMRPD2J0041) for research support. Mass spectrometry analyses were performed by the Mass Spectrometry Facility of the Institute of Chemistry, Academia Sinica.

■ REFERENCES

(1) Kim, H.-S.; Lee, C.-R.; Im, J.-H.; Lee, K.-B.; Moehl, T.; Marchioro, A.; Moon, S.-J.; Humphry-Baker, R.; Yum, J.-H.; Moser, J. E.; Grätzel, M.; Park, N.-G. Lead Iodide Perovskite Sensitized All-Solid-State Submicron Thin Film Mesoscopic Solar Cell with Efficiency Exceeding 9%. *Sci. Rep.* **2012**, *2*, No. 591.

(2) Dong, Q.; Fang, Y.; Shao, Y.; Mulligan, P.; Qiu, J.; Cao, L.; Huang, J. Electron-Hole Diffusion Lengths> 175 μm in Solution-Grown CH3NH3PbI3 Single Crystals. *Science* **2015**, *347*, 967−970.

(3) Stranks, S. D.; Eperon, G. E.; Grancini, G.; Menelaou, C.; Alcocer, M. J. P.; Leijtens, T.; Herz, L. M.; Petrozza, A.; Snaith, H. J. Electron-Hole Diffusion Lengths Exceeding 1 Micrometer in an Organometal Trihalide Perovskite Absorber. *Science* **2013**, *342*, 341−344.

(4) Xing, G.; Mathews, N.; Sun, S.; Lim, S. S.; Lam, Y. M.; Grätzel, M.; Mhaisalkar, S.; Sum, T. C. Long-Range Balanced Electron- and Hole-Transport Lengths in Organic-Inorganic $CH_3NH_3PbI_3$. *Science* **2013**, *342*, 344−347.

(5) Kojima, A.; Teshima, K.; Shirai, Y.; Miyasaka, T. Organometal Halide Perovskites as Visible-Light Sensitizers for Photovoltaic Cells. *J. Am. Chem. Soc.* **2009**, *131*, 6050−6051.

(6) Yang, W. S.; Park, B. W.; Jung, E. H.; Jeon, N. J.; Kim, Y. C.; Lee, D. U.; Shin, S. S.; Seo, J.; Kim, E. K.; Noh, J. H.; Seok, S. I. Iodide Management in Formamidinium-Lead-Halide−Based Perovskite Layers for Efficient Solar Cells. *Science* **2017**, *356*, 1376−1379.

(7) Zhang, F.; Wang, S. R.; Li, X. G.; Xiao, Y. Recent Progress of Perovskite Solar Cells. *Curr. Nanosci.* **2016**, *12*, 137−156.

(8) Jiang, Q.; Zhao, Y.; Zhang, X.; Yang, X.; Chen, Y.; Chu, Z.; Ye, Q.; Li, X.; Yin, Z.; You, J. Surface passivation of perovskite film for efficient solar cells. Surface Passivation of Perovskite Film for Efficient Solar Cells. *Nat. Photonics* **2019**, *13*, 460−466.

(9) Kim, M.; Kim, G.-H.; Lee, T. K.; Choi, I. W.; Choi, I. W.; Jo, Y.; Yoon, Y. J.; Kim, J. W.; Lee, J.; Huh, D.; Lee, H.; Kwak, S. K.; Kim, J. Y.; Kim, D. S. Methyl Ammonium Chloride Induces Intermediate Phase Stabilization for Efficient Perovskite Solar Cells. *Joule* **2019**, *3*, 2179−2192.

(10) Jung, E. H.; Jeon, N. J.; Park, E. Y.; Moon, C. S.; Shin, T. J.; Yang, T.-Y.; Noh, J. H.; Seo, J. Efficient, Stable and Scalable Perovskite Solar Cells Using Poly (3-hexylthiophene). *Nature* **2019**, *567*, 511−515.

(11) Anaraki, E. H.; Kermanpur, A.; Steier, L.; Domanski, K.; Matsui, T.; Tress, W.; Saliba, M.; Abate, A.; Grätzel, M.; Hagfeldt, A.; Correa-Baena, J.-P. Highly Efficient and Stable Planar Perovskite Solar Cells by Solution-Processed Tin Oxide. *Energy Environ. Sci.* **2016**, *9*, 3128−3134.

(12) Saliba, M.; Orlandi, S.; Matsui, T.; Aghazada, S.; Cavazzini, M.; Correa-Baena, J.-P.; Gao, P.; Scopelliti, R.; Mosconi, E.; Dahmen, K.-H.; Angelis, F. D.; Abate, A.; Hagfeldt, A.; Pozzi, G.; Grätzel, M.; Nazeeruddin, M. K. A molecularly Engineered Hole-Transporting Material for Efficient Perovskite Solar Cells. *Nat. Energy* **2016**, *1*, No. 15017.

(13) Lee, O. P.; Yiu, A. T.; Beaujuge, P. M.; Woo, C. H.; Holcombe, T. W.; Millstone, J. E.; Douglas, J. D.; Chen, M. S.; Fréchet, J. M. J. Efficient Small Molecule Bulk Heterojunction Solar Cells with High Fill Factors via Pyrene-Directed Molecular Self-Assembly. *Adv. Mater.* **2011**, *23*, 5359−5363.

(14) Christians, J. A.; Fung, R. C. M.; Kamat, P. V. An Inorganic Hole Conductor for Organo-Lead Halide Perovskite Solar Cells. Improved Hole Conductivity with Copper Iodide. *J. Am. Chem. Soc.* **2014**, *136*, 758−764.

(15) Qin, P.; Tanaka, S.; Ito, S.; Tetreault, N.; Manabe, K.; Nishino, H.; Nazeeruddin, M. K.; Grätzel, M. Inorganic Hole Conductor-Based Lead Halide Perovskite Solar Cells with 12.4% Conversion Efficiency. *Nat. Commun.* **2014**, *5*, No. 3834.

(16) Hu, Z.; Fu, W.; Yan, L.; Miao, J.; Yu, H.; He, Y.; Goto, O.; Meng, H.; Chen, H.; Huang, W. Effects of Heteroatom Substitution in Spiro-Bifluorene Hole Transport Materials. *Chem. Sci.* **2016**, *7*, 5007−5012.

(17) Chen, H.; Fu, W.; Huang, C.; Zhang, Z.; Li, S.; Ding, F.; Shi, M.; Li, C.-Z.; Jen, A. K. Y.; Chen, H. Molecular Engineered Hole-Extraction Materials to Enable Dopant-Free, Efficient p-i-n Perovskite Solar Cells. *Adv. Energy Mater.* **2017**, *7*, No. 1700012.

(18) Xu, B.; Zhang, J.; Hua, Y.; Liu, P.; Wang, L.; Ruan, C.; Li, Y.; Boschloo, G.; Johansson, E. M. J.; Kloo, L.; Hagfeldt, A.; Jen, A. K. Y.; Sun, L. Tailor-Making Low-Cost Spiro[fluorene-9,9′-xanthene]-Based 3D Oligomers for Perovskite Solar Cells. *Chem* **2017**, *2*, 676−687.

(19) Bi, D.; Xu, B.; Gao, P.; Sun, L.; Grätzel, M.; Hagfeldt, A. Facile Synthesized Organic Hole Transporting Material for Perovskite Solar Cell with Efficiency of 19.8%. *Nano Energy* **2016**, *23*, 138−144.

(20) Xu, B.; Bi, D.; Hua, Y.; Liu, P.; Cheng, M.; Grätzel, M.; Kloo, L.; Hagfeldt, A.; Sun, L. A Low-Cost Spiro[Fluorene-9,9′-Xanthene]-Based Hole Transport Material for Highly Efficient Solid-State Dye-Sensitized Solar Cells and Perovskite Solar Cells. *Energy Environ. Sci.* **2016**, *9*, 873−877.

(21) Huang, C.; Fu, W.; Li, C.-Z.; Zhang, Z.; Qiu, W.; Shi, M.; Heremans, P.; Jen, A. K. Y.; Chen, H. Dopant-Free Hole-Transporting Material with A C_3h Symmetrical Truxene Core for Highly Efficient Perovskite Solar Cells. *J. Am. Chem. Soc.* **2016**, *138*, 2528−2531.

(22) Guan, L.; Yin, X.; Zhao, D.; Wang, C.; An, Q.; Yu, J.; Shrestha, N.; Grice, C. R.; Awni, R. A.; Yu, Y.; Song, Z.; Zhou, J.; Meng, W.; Zhang, F.; Ellingson, R. J.; Wang, J.; Tang, W.; Yan, Y. Cost-Effective Hole Transporting Material for Stable and Efficient Perovskite Solar Cells with Fill Factors up to 82%. *J. Mater. Chem. A* **2017**, *5*, 23319−23327.

(23) Molina-Ontoria, A.; Zimmermann, I.; Garcia-Benito, I.; Gratia, P.; Roldán-Carmona, C.; Aghazada, S.; Grätzel, M.; Nazeeruddin, M. K.; Martín, N. Benzotrithiophene-Based Hole-Transporting Materials for 18.2% Perovskite Solar Cells. *Angew. Chem., Int. Ed.* **2016**, *55*, 6270−6274.

(24) Rakstys, K.; Saliba, M.; Gao, P.; Gratia, P.; Kamarauskas, E.; Paek, S.; Jankauskas, V.; Nazeeruddin, M. K. Highly Efficient Perovskite Solar Cells Employing an Easily Attainable Bifluorenylidene-Based Hole-Transporting Material. *Angew. Chem., Int. Ed.* **2016**, *55*, 7464−7468.

(25) Lin, Y.-D.; Ke, B.-Y.; Lee, K.-M.; Chang, S. H.; Wang, K.-H.; Huang, S. H.; Wu, C.-G.; Chou, P.-T.; Jhulki, S.; Moorthy, J. N.; Chang, Y. J.; Liau, K.-L.; Chung, H.-C.; Liu, C.-Y.; Sun, S.-S.; Chow, T. J. Hole-Transporting Materials Based on Twisted Bimesitylenes for Stable Perovskite Solar Cells with High Efficiency. *ChemSusChem* **2016**, *9*, 274−279.

(26) Lin, Y.-S.; Abate, S. Y.; Lai, K.-W.; Chu, C.-W.; Lin, Y.-D.; Tao, Y.-T.; Sun, S.-S. New Helicene-type Hole-transporting Molecules for

High Efficiency and Durable Perovskite Solar Cells. *ACS Appl. Mater. Interfaces* **2018**, *10*, 41439−41449.
(27) Rezaee, E.; Liu, X.; Hu, Q.; Dong, L.; Chen, Q.; Pan, J.-H.; Xu, Z.-X. Dopant-Free Hole Transporting Materials for Perovskite Solar Cells. *Sol. RRL* **2018**, *2*, No. 1800200.
(28) Hu, Q.; Rezaee, E.; Dong, Q.; Shan, H.; Chen, Q.; Wang, L.; Liu, B.; Pan, J.-H.; Xu, Z.-X. P3HT/Phthalocyanine Nanocomposites as Efficient Hole-Transporting Materials for Perovskite Solar Cells. *Sol. RRL* **2019**, *3*, No. 1800264.
(29) Matthews, J. R.; Niu, W.; Tandia, A.; Wallace, A. L.; Hu, J.; Lee, W. Y.; Giri, G.; Mannsfeld, S. C. B.; Xie, Y.; Cai, S.; Fong, H. H.; Bao, Z.; He, M. Scalable Synthesis of Fused Thiophene-Diketopyrrolopyrrole Semiconducting Polymers Processed from Nonchlorinated Solvents into High Performance Thin Film Transistors. *Chem. Mater.* **2013**, *25*, 782−789.
(30) Chung, J. W.; Park, W.-T.; Park, J.-Il.; Yun, Y.; Gu, X.; Lee, J.; Noh, Y.-Y. Thiophene-Thiazole-Based Semiconducting Copolymers for High-Performance Polymer Field-Effect Transistors. *ACS Appl. Mater. Interfaces* **2017**, *9*, 38728−38736.
(31) Dang, D.; Zhou, P.; Wu, Y.; Xu, Y.; Zhi, Y.; Zhu, W. Isomeric Organic Semiconductors Containing Fused-Thiophene Cores: Molecular Packing and Charge Transport. *Phys. Chem. Chem. Phys.* **2018**, *20*, 13171−13177.
(32) Tan, L.; Zhang, L.; Jiang, X.; Yang, X.; Wang, L.; Wang, Z.; Li, L.; Hu, W.; Shuai, Z.; Li, L.; Zhu, D. A Densely and Uniformly Packed Organic Semiconductor Based on Annelated β-Trithiophenes for High-Performance Thin Film Transistors. *Adv. Funct. Mater.* **2009**, *19*, 272−276.
(33) Shi, J.; Li, Y.; Jia, M.; Xu, L.; Wang, H. Organic Semiconductors Based on Annelated β-Oligothiophenes and Its Application For Organic Field-Effect Transistors. *J. Mater. Chem.* **2011**, *21*, 17612−17614.
(34) Zhao, R.; Min, Y.; Dou, C.; Liu, J.; Wang, L. A New Electron-Rich Unit for Polymer Electron Acceptors: 4,4-Difluoro-4H-Cyclopenta[2,1-b:3,4-b′]Dithiophene. *Chem. - Eur. J.* **2017**, *23*, 9486−9490.
(35) Li, H.; Koh, T. M.; Hao, Y.; Zhou, F.; Abe, Y.; Su, H.; Hagfeldt, A.; Grimsdale, A. C. Comparative Studies on Rigid π Linker-Based Organic Dyes: Structure−Property Relationships and Photovoltaic Performance. *ChemSusChem* **2014**, *7*, 3396−3406.
(36) Kim, J. S.; Fei, Z.; Wood, S.; James, T. D.; Sim, M.; Cho, K.; Heeney, M. J.; Kim, J.-S. Germanium- and Silicon-Substituted Donor−Acceptor Type Copolymers: Effect of The Bridging Heteroatom on Molecular Packing and Photovoltaic Device Performance. *Adv. Energy Mater.* **2014**, *4*, No. 1400527.
(37) Ie, Y.; Nitani, M.; Ishikawa, M.; Nakayama, K.-I.; Tada, H.; Kaenda, T.; Aso, Y. Electronegative Oligothiophenes for N-Type Semiconductors: Difluoromethylene-Bridged Bithiophene and Its Oligomers. *Org. Lett.* **2007**, *9*, 2115−2118.
(38) Franckevičius, M.; Mishra, A.; Kreuzer, F.; Luo, J.; Zakeeruddin, S. M.; Grätzel, M. A Dopant-Free Spirobi[cyclopenta-[2,1-b:3,4-b′]-dithiophene] Based Hole-Transport Material for Efficient Perovskite Solar Cells. *Mater. Horiz.* **2015**, *2*, 613−618.
(39) Ma, S.; Zhang, H.; Zhao, N.; Cheng, Y.; Wang, M.; Shen, Y.; Tu, G. Spiro-Thiophene Derivatives as Hole-Transport Materials for Perovskite Solar Cells. *J. Mater. Chem. A* **2015**, *3*, 12139−12144.
(40) Caliò, L.; Kazim, S.; Salado, M.; Zimmermann, I.; Nazeeruddin, M. K.; Ahmad, S. Design of Cyclopentadithiophene-Based Small Organic Molecules as Hole Selective Layers for Perovskite Solar Cells. *Sustainable Energy Fuels* **2018**, *2*, 2179−2186.
(41) Lee, K.-M.; Chen, K.-S.; Wu, J.-R.; Lin, Y.-D.; Yu, S.-M.; Chang, S. H. Highly Efficient and Stable Semi-Transparent Perovskite Solar Modules with A Trilayer Anode Electrode. *Nanoscale* **2018**, *10*, 17699−17704.
(42) Lin, Y.-D.; Lee, K.-M.; Ke, B.-Y.; Chen, K.-S.; Cheng, H.-C.; Lin, W.-J.; Chang, S. H.; Wu, C.-G.; Kuo, M.-C.; Chung, H.-C.; Chou, C.-C.; Chen, H.-Y.; Liau, K.-L.; Chow, T. J.; Sun, S.-S. Rational Design of Cyclopenta[2,1-b;3,4-b′]dithiophene-bridged Hole Transporting Materials for Highly Efficient and Stable Perovskite Solar Cells. *Energy Technol.* **2019**, *7*, 307−316.
(43) Sun, Y.; Tan, L.; Jiang, S.; Qian, H.; Wang, Z.; Yan, D.; Di, C.; Wang, Y.; Wu, W.; Yu, G.; Yan, S.; Wang, C.; Hu, W.; Liu, Y.; Zhu, D. High-Performance Transistor Based on Individual Single-Crystalline Micrometer Wire of Perylo[1,12-b,c,d]thiophene. *J. Am. Chem. Soc.* **2007**, *129*, 1882−1883.
(44) Xu, B.; Sheibani, E.; Liu, P.; Zhang, J.; Tian, H.; Vlachopoulos, N.; Boschloo, G.; Kloo, L.; Hagfeldt, A.; Sun, L. Carbazole-Based Hole-Transport Materials for Efficient Solid-State Dye-Sensitized Solar Cells and Perovskite Solar Cells. *Adv. Mater.* **2014**, *26*, 6629−6634.
(45) Li, S.; Yang, X.; Qu, D.; Wang, W.; Wang, Y.; Sun, L. Molecular Design of D-π-A Type II Organic Sensitizers for Dye Sensitized Solar Cells. *Chin. J. Chem.* **2012**, *30*, 2315−2321.
(46) Kumaresan, P.; Vegiraju, S.; Ezhumalai, Y.; Yau, S. L.; Kim, C.; Lee, W.-H.; Chen, M.-C. Fused-Thiophene Based Materials for Organic Photovoltaics and Dye-Sensitized Solar Cells. *Polymers* **2014**, *6*, 2645−2669.
(47) Zheng, A.; Ren, M.; Zhang, Y.; Cai, Y.; Zhang, J.; Yuan, Y.; Lei, M.; Wang, P. A Thioxanthenothioxanthene-based Hole Transporter with 2D Molecular Stacking for Efficient and Thermostable Perovskite Solar Cells. *ACS Mater. Lett.* **2020**, *2*, 691−698.

https://doi.org/10.1021/acsaem.1c00328
ACS Appl. Energy Mater. 2021, 4, 4719−4728